Automotive and Engine Technology (2021) 6:219–234
https://doi.org/10.1007/s41104-021-00088-z

ORIGINAL PAPER

Aging investigations and consideration for automotive high power lithium-ion batteries in a 48 V mild hybrid operating strategy

D. Geringer[1] · P. Hofmann[1] · J. Girard[2] · E. Trunner[2] · W. Knefel[2]

Received: 21 December 2020 / Accepted: 11 August 2021 / Published online: 2 September 2021

Abstract

This paper focuses on the battery aging of automotive high power lithium-ion batteries intended for 48 V mild hybrid systems. Due to a long vehicle lifetime, battery aging is of high importance, and its consideration within a hybrid system is crucial to ensure a sufficient lifetime for the battery. At the moment, only a few aging investigations and models specifically for automotive high power cells are available. Consequently, all present aging consideration methods are based on the few published aging models focusing on consumer cells. This paper describes the development of an aging model for automotive high power cells and the integration into a mild hybrid operating strategy to actively control the battery aging process during its operation. The underlying aging investigations of high-power battery cells are shown to analyze the main influences of temperature, state of charge, and C-rate. These tests are used to develop the aging model, capable of considering the main influences on the aging process. Based on this model and all gained insights, different methods for considering battery aging in a mild hybrid system are investigated. The goal is to control the aging process during operation and consequently decrease the negative influence. Two active intervention methods are developed and integrated into a 48 V mild hybrid operating strategy to validate their potential. It is possible to control the aging process and at the same time to use the insights for improving the basic hybrid powertrain design regarding reduced aging and battery costs.

Keywords High power lithium-ion battery · Battery aging · Aging model · Liquid cooling · Mild hybrid system · 48 V · Operating strategy

Abbreviations

CCCV	Constant current constant voltage
DC	Direct current
DoD	Depth of discharge
ECMS	Equivalent cost consumption strategy
ECU	Engine control unit
EM	Electric motor
LLI	Loss of lithium inventory
NTC	Negative temperature coefficient
SEI	Solid electrolyte interphase
SI	Spark-ignition
SoC	State of charge
SoH	State of heath
WLTC	Worldwide harmonized light-duty vehicles test cycle

✉ D. Geringer
dominik.geringer@tuwien.ac.at

[1] Institute for Powertrains and Automotive Technology, Vienna University of Technology, Getreidemarkt 9, 1060 Vienna, Austria

[2] Robert Bosch AG, Göllnergasse 15-17, 1030 Vienna, Austria

1 Introduction

Future CO_2-emission limits and therefore fuel consumption targets for vehicle manufacturers are quite challenging. Fleet consumption levels have to be reduced significantly in order to meet the mandatory goals. One common way is increasing the electrification of conventional powertrains towards hybrid and battery electric vehicles. Especially mild hybrid systems with an on-board electrical supply voltage of 48 V represent a promising technology approach for a fast and widespread implementation. They achieve substantial fuel consumption savings at lower costs compared to high voltage hybrid electric vehicles or plug-in hybrid vehicles [5, 9, 27]. These mild hybrid powertrains consist of a small electric motor capable of assisting the combustion engine during acceleration (boosting) or recuperating

energy during braking events. The peak power of the electric motor in 48 V-systems is usually about 8–15 kW, correlating to currents of 150–300 A [9]. The energy storage is a 48 V-lithium-ion battery pack with a smaller capacity to reach an attractive cost-to-benefit ratio. This results in high C-rates only delivered properly by lithium-ion cells specially designed for high specific power output. The lithium diffusion time between the electrodes is shortened at these cells due to, for example, a thinner active material, an increased active electrode surface, and a higher porosity. The main approach is reducing the lithium storage material dimensions and enhancing the electrochemical performance. Possible ways are for example carbon coating [6, 7], metal doping [16], and particle size reduction of the lithium storage material into the nanometer range [10, 17] or using carbon nanotubes [12]. This tailoring to high specific power results in a low resistance, high possible charge rates, and lower specific energy.

Although the resistance only has small values, it has a decisive influence on the time to reach the voltage cut-off and the heat production at high currents (high C-rates). Especially at higher C-rates, the temperature distribution across the cell is very inhomogeneous because of the layered cell structure with the isolating separator between the electrodes. This results in a hotter core and a cooler case. An example is shown in the study by Lundgren [15]. This thermal distribution is also challenging for the temperature simulation of cells and their use in aging calculations regarding the aging-relevant temperature. Thermal models are needed for determining a representative core temperature because a direct measurement is usually not possible. Lumped mass models using a block of unified material and the thermal in- and outputs are suitable for most applications.

The overall aging of lithium-ion batteries consists of two different aging types, the calendar and the cycle aging. These aging types represent the summation of different aging mechanisms like loss of active material, loss of lithium inventory (LLI), pore clogging or solid electrolyte interphase (SEI) growth. These mechanisms cause a deterioration of the battery performance with a capacity loss and resistance rise. Calendar aging is a known effect occurring continuously. Many different aging mechanisms are happening here, but the main reason is the growth of the SEI-layer with a loss of lithium inventory with a loss of the cell capacity. Based on numerous studies [1, 3, 4, 25] it depends mainly on time, temperature, and state of charge (SoC). The second aging type, cycle aging, results from different aging mechanisms during charging and discharging. It differs by conditions of the temperature and mean state of charge [25]. The common understanding is that the cycle aging is influenced mainly by the height of charging cycles (depth of discharge DoD), the absolute state of charge, temperature, and the charge rate (C-rate) [8]. The resulting overall battery aging is the sum of the calendar and cycle aging. The lifetime of batteries is an important aspect for automotive applications because it should last as long as the cars lifetime (> 10 years). This is much longer than in most consumer applications like smartphones or power tools [22]. At the moment, most publications are focusing exclusively on high energy cells. Some papers target high power cells, but most of these investigations concentrate on consumer applications, e.g., Wang [28]. Still, only a few center on automotive power cells with a much higher capacity and geometric dimensions than consumer cells. For this reason, the investigation in this paper will focus on such automotive power cells to research battery aging and its main influences. Cell tests deliver data to develop an aging model capable of calculating the actual aging state.

The developed aging model will consider and control the battery aging in a hybrid system operating strategy during the system operation. In general, these strategies calculate the optimal distribution between both power sources (fuel and battery) in a hybrid vehicle at any time. A commonly used method and the basis for the investigations is the equivalent cost consumption strategy (ECMS). The main idea behind the ECMS is that electric energy in an autarkical hybrid vehicle only originates from the consumed fuel and can be converted to fuel consumption with an equivalent factor. An optimization function searches for the best torque distribution between the electric motor and the internal combustion engine. A so-called cost function calculates the overall costs of various torque distributions (equivalent fuel consumption) at any time step. In a simple ECMS-version, the equivalent factor is only dependent on the state of charge. This parameter solely controls the torque distribution to reach a charge sustaining mode for the hybrid vehicle. Battery aging is rarely focused on in existing operating strategy approaches. The main goal is often exclusively to reduce fuel consumption and emissions within the constraints of the battery current or power limits.

Some existing strategies can consider battery aging by using a concept of severity maps in models using the cumulative charge throughput as an end-of-life criterion. Ambient conditions causing faster aging lead to higher severity factors for the actual charge throughput, and these areas will be avoided by the optimization more often. This method is described in different publications, e.g. [23, 24]. Other possible consideration methods use Neuronal Networks [14] or Pareto optimization to avoid high temperatures with an electrochemical battery model [18]. However, all of these methods are based on the few available high power cell aging models designed for smaller consumer cells as described in [28] or use a global optimization strategy (known driving path required). Therefore, the second scope of this investigation is to consider the battery aging during operation and control the aging process by a new developed hybrid

electric vehicle-operating strategy. Two different methods are developed and tested.

2 Methodology

2.1 Aging investigations

The aging investigations are intended to speed up the long-lasting aging process of lithium-ion cells. This is done by elevating the batteries' stress conditions (e.g., higher ambient temperature) during tests. All performed measurements are separated according to the aging types into calendar aging measurements and cyclic charging/discharging tests at different conditions. The aging test bench consists of several battery testing channels, one for each cell, and the conditioning system.

2.1.1 Measurement setup

The batteries used for the tests are high power lithium-ion cells with a capacity of about 8 Ah and a maximum C-rate of over 35 C. During the aging investigations, the full capacity is used for the determination of the maximal SoC. In automotive use, the usable capacity of the cell is usually smaller to limit aging. The cells electrodes are a cathode of lithium–nickel–manganese–cobalt–oxide (NMC) and a graphite-anode. These cells are designed for automotive applications of 48 V hybrid electric vehicles. At all testing conditions during this investigation, the cells stay within the normal operating limits according to the datasheet, so no overcharging or deep discharging occurs. The cells are clamped with stainless steel plates to control the expansion of prismatic cells and maintain the specified cell width according to the datasheet of the producer, see Fig. 1. An expansion would lead to additional aging due to connection losses between the electrode material and the current collector [3, 11]. Furthermore, an aluminum plate for a better heat transfer from the case to the liquid cooling fluid is part of the mounting.

A negative temperature coefficient (NTC)-thermistor measured the cell temperature at the top of the case between both electrodes. At higher charge rate tests in addition to this case measurement also the electrode temperature was measured with a NTC-sensor at the current collectors directly on the cell terminal. The electrodes have a good thermal connection due to the current collector's metallic contact to the layers. This additional information helps to estimate the core temperature and the thermal distribution inside the cell.

Maintaining the same battery temperature is essential for accurate data, especially during tests with high currents causing cell heating in the charging and discharging phases. Hence, a cooling and conditioning system is necessary for

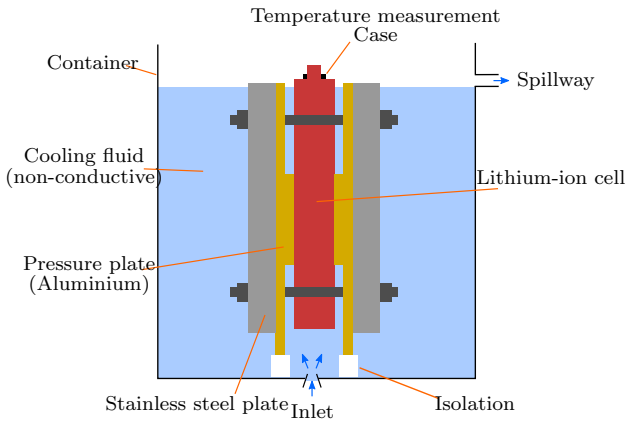

Fig. 1 Direct cooling and mounting system of one cell during the investigations

the measurements to dissipate the heat. Due to the strong heating and small surface area at high C-rate tests, a liquid-cooling system was used because an air-cooling system is insufficient. The cooling system utilizes a separate liquid bath for each lithium-ion cell, where it is immersed in the cooling liquid (Fig. 1). The fluid is a non-conductive water-glycol mixture with a level just beneath the electrode terminals. The baths are integrated into fluid circuits of the temperature-conditioning system. Four similar circuits, one for each testing temperature (5, 25, 35 and 50°C) are used and each one offers a separate temperature setting with a maximum tolerance of ±1°C. This direct fluid cooling system allows a constant ambient temperature and a huge reduction of the otherwise necessary cooling pause during the high C-rates cycling.

2.1.2 Test procedure

The main focus of the investigations are the aging influences of temperature and charge rate. The effect of the state of charge is also analyzed. In addition, a specific test determines the representative temperature (aging-relevant temperature) for the aging model.

2.1.3 Temperature and charge rate influence

The calendar aging tests are conducted at defined constant conditions. Different temperature levels and a constant state of charge with 50% (constant voltage) are used during the storage investigations. These tests are aimed at parameterizing a model according to the well-known Arrhenius equation to describe the temperature dependence of the chemical reactions. The general equation must be extended by the aging time to calculate the calendrical degradation of cells [1, 3, 26] and is used in numerous similar aging investigations [28]. The storage tests were run with just one cell

per ambient temperature to have more cells available for the cycling tests.

On the other hand, cycle aging tests simulate the usage of a battery cell by charging/discharging them at different conditions. The goal is to determine the current and temperature influence on the battery aging for these high power lithium-ion cells during operation. So, the cells were cycled at different ambient temperatures and C-rates to test these influences. To limit the possible combinations, only one mean state of charge of 50% and one depth of discharge (DoD, the difference between SoC high and low) of 10% was used for these tests, resulting in a SoC range of 45–55%. All conditions were derived from a typical mild hybrid electric vehicle application [9, 22]. The tests were conducted with two battery cells at each condition to account for variability between cell characteristics in manufacturing. The test matrix for the different conditions is shown in Table 1. This plan limits the needed amount of cells at a full factorial test but maintains at least three tests per C-rate and temperature. The C-rates range from 0 C, the calendar aging tests, to a maximum of 25 C, approximately the rate during boosting and recuperation maneuvers. The temperature range spans from 5 to 50°C and covers four different levels. 25°C represents the normal ambient temperature, where no accelerated aging is happening, and it is also the rated temperature for charging according to the cell datasheet. The 25 C and 5°C condition checks for lithium plating (occurs mainly charging at low temperature and high C-rates), where the metallic lithium deposits at the anode and could lead to rapid aging or even an internal short circuit because of forming dendrites [13].

The test cycle consists of three phases with a charging period followed by a discharging period of equal length and a cooling pause to regain its starting temperature at the end of a full cycle. The C-rates the same for charging and discharging. The last phase for cooling ranges from 0 min at 1 C and 3 C to 12 min for the 25 C-tests. The cycle pause is used to reach the same starting temperature for all C-rates and is based on initial measurements. This phase is heavily dependent on the used cooling system. The pause period is also varied during a separate investigation at a high C-rate test to find the aging-relevant cell temperature for the aging model.

Table 1 Test matrix for the aging investigations on high power lithium-ion cells at 50% mean SoC and 10% DoD for the cycling tests

Temperature (°C)	0 C	1 C	3 C	10 C	25 C
5	x	x	x	x	x
25	x	x	x	x	
35	x		x	x	x
50	x	x			x

The aging state is monitored through recurrent weekly checkup cycles measuring the capacity and resistance after conditioning all cells at a temperature of 25°C. A standard constant-current constant-voltage (CCCV) procedure is used to charge and discharge the cell to determine the capacity with a measurement of the charge throughput. The charge rate at the constant current phase is 1 C until reaching a voltage of 4.15 V. The charge continues at this constant voltage until the current falls below a 100 mA-threshold (about 0.01 C). Afterward, the charge and discharge direct current (DC)-resistances are calculated with Ohms law using the voltage drop after 10 s at a fixed current pulse of 3 C. This calculation is done once at the standard temperature 25°C and once at the measurement temperature of each cell.

2.1.4 State of charge influence

For investigating the state of charge influence, several storage tests at different SoC-levels are conducted with only one cell at each condition. The SoC-level for each tested cell is ranging from 10 to 90% in 20% steps plus a fully charged cell. These investigations do not require a cell cooling and are conducted at room temperature (23°C).

2.1.5 Aging-relevant cell temperature

At a high C-rate, the thermal distribution inside a cell is very inhomogeneous due to its inner layered structure. The core is most likely hotter than the surface. For the use in an aging model, a representative temperature governing the aging process must be determined with a separate test. If the aging is mainly temperature-dependent, it will be faster at higher temperatures. Shorter cooling phases could achieve such a temperature increase during a cycle, which is done in this separated test. At the initial test, the pause for 10 C tests is very long so that the cell could reach its starting electrode temperature at every cycle. Because of that pause, the cell rests up to about 90% of the cycle time. The pause time for the cell cooling during a high C-rate test is shortened in two steps in this test to increase the mean temperature of the cell. The resulting aging process of each variation step is then analyzed and compared to the equivalent capacity loss according to the Arrhenius aging model in the same step using the higher battery core temperature. Because no core temperature measurement is possible, the determination is done by using a thermal simulation model. It calculates the core temperature for the cell according to the actual usage. This simulation is based on a lumped mass model (Eq. (1)), which calculates the temperature with a thermal balance of the lumped mass (battery):

$$\dot{Q}_{\text{gen}} = m_{\text{Core}} \cdot c_{\text{Core}} \cdot \frac{\partial T_{\text{Core}}}{\partial t} + k \cdot A \cdot (T_{\text{Core}} - T_{\text{Case}}) \quad (1)$$

with $\dot{Q}_{\text{gen}}$ is the rate of the heat generation in W, m_{Core} is the mass of the cell core in kg, c_{Core} is the specific heat capacity of the core in J kg^{-1} K^{-1}, T_{Core} is the temperature of the cell core in K, T_{Case} is the temperature of the cell case in K, k is the heat transfer coefficient in W m^{-2} K^{-1}, A is the heat transfer surface area in m^2.

In this equation, the left side describes all heat generation. There are many possible sources of heat generation [2, 20] including the electrical and ionic resistance in the cells' active mass and electrolyte. These sources can be summarized to the DC resistance of the cell. Minor contribution to the heat generation is also made by other polarization effects not covered by the DC resistance, but they can be neglected for simplification. During the investigations, only the heat generation according to the DC-resistance is used. The right side of the equation shows the internal energy change corresponding to the temperature increase and the dissipating heat from the lumped mass/battery dependent on the cooling. For more accurate modeling of the core temperature, also the aluminum case itself has to be taken into account, using Eq. (1) as well. Thereby, the poor heat transfer from the core to the case due to the electrical and thermal insulation between them must be considered.

2.2 Aging considerations in a hybrid powertrain

The aging consideration in a hybrid system can be done in two different ways, either actively during operation or prior to the use at the design stage of the hybrid powertrain. Both possibilities will be investigated in this paper, but the main focus is on the consideration during hybrid system operation. This is aimed at reaching the ability to control battery's aging process and maintain a defined lifetime. Possible ways are interventions of the operating strategy to avoid areas with high aging during battery operation to ideally maintain the desired lifetime and simultaneously achieve high fuel savings over the whole lifetime. The second possible method to consider battery aging in a hybrid system is at the basic powertrain design. This works by changing certain parameters (e.g., state of charge) or component dimensions like a battery capacity reduction. Altogether two separate active considerations integrated into the operating strategy and various powertrain design improvements are shown in this paper.

2.2.1 Consideration of the battery aging during operation

Two different approaches are developed and tested to gain the ability to control the aging process. Both use different kinds of interventions to limit the use and, therefore, aging in certain situations with fast aging to avoid exceeding the expected battery degradation. Each presented method is validated on an engine test bench, and the potential is assessed in this paper.

– Method A: aging integration into the ECMS cost function. The first developed variant integrates the battery aging directly into the cost function of an ECMS operating strategy, the first line of Eq. (2). It sums up the overall equivalent fuel mass flow of both power systems. $P_{\text{eqv, ICE}}$ is the equivalent power of the fuel (chemical energy) calculated with the fuel mass flow, the lower heating value, and the actual engine load point. The equivalent power of the electric motor is $P_{\text{eqv, EM}}$. It uses the electric power of the motor P_{EM} and an equivalence factor s. All equivalent power values are usually called costs. The integration of the aging into the cost function is a similar approach to the severity maps of Suri and Serrao [23, 24] except that in the now proposed method, no end of life criteria based on a fixed limit for the charge throughput is used. Instead, additional equivalent costs based on aging (P_{Aging}) are added to the electrical costs in the general cost calculation of the ECMS at every time step. Equation (2) shows the adapted cost function for consideration of the battery aging into the operating strategy. The operating strategy searches for the lowest overall costs at each time step and will most likely avoid areas of high aging, for example, during boosting events at high ambient temperatures.

$$\begin{aligned} P_{\text{eqv, tot}}(t) =& P_{\text{eqv, ICE}}(t) + P_{\text{eqv, EM}}(t) \\ =& P_{\text{eqv, ICE}}(t) + \left[s(\text{SoC}) + s(\text{Aging})\right] \cdot P_{\text{EM}}(t) \end{aligned} \quad (2)$$

$$\begin{aligned} P_{\text{Aging}} =& s(\text{Aging}) \cdot P_{\text{EM}}(t) = \text{Fac}_{\text{dT}}(I_{\text{act}}) \cdot \text{Fac}_{\text{Amb}} \\ & \cdot \text{Fac}_{\text{SoH}} \cdot P_{\text{EM}}(t) \end{aligned} \quad (3)$$

with $P_{\text{eqv, tot}}(t)$ are the total equivalent energy costs in W, $P_{\text{eqv, ICE}}(t)$ are the ICE energy costs in W, $P_{\text{eqv, EM}}(t)$ are the electrical equivalent costs in W, $P_{\text{EM}}(t)$ is the electric motor power in W, s(SoC) is the equivalence factor dependent of the SoC, s(Aging) is the equivalence factor dependent of aging, P_{Aging} are the energy costs for aging in W, $\text{Fac}_{\text{dT}}(I_{\text{act}})$ is the temperature rise factor, Fac_{Amb} is the ambient temperature factor, Fac_{SoH} is the SoH difference factor.

The challenge in this approach is finding a suitable aging-dependent equivalence factor s_{Aging}. This parameter needs a calculation of the aging effect on fuel consumption and will be complex. A simple approach is used to test this method by referencing the aging costs to the overall costs with different factors to react to changes of the operating parameters. The added aging costs are calculated with Eq. (3) and use the temperature rise in the

battery due to the operation of the electric motor for gaining equivalent aging costs. In this equation, high electric motor torques (e.g., during boosting) lead to high temperature rises with following faster aging and higher aging costs represented by the factor $\mathrm{Fac}_{\mathrm{dT}}$. Because aging is dependent on the absolute temperature, an additional factor $\mathrm{Fac}_{\mathrm{Amb}}$ is considering the ambient temperature for penalizing warm and cold climates. This factor is also crucial regarding lithium plating for charging events at low temperatures (favorable conditions for lithium plating). The third factor $\mathrm{Fac}_{\mathrm{SoH}}$ is dependent on the deviation between the actual aging state to the planned state of health (SoH). This parameter allows the possibility of active control of the aging process. During the test bench measurements, this value is varied. For the integration into the operating strategy, the aging costs are designed to be nearly 0 at normal operation and around 30% of the electric energy costs at higher aging potentials (assuming a variation factor $\mathrm{Fac}_{\mathrm{SoH}}$ of 1). This assumption results from a prior offline calculation and describes a reasonable level for the starting parameters at the test bench measurements. If the aging factor and, therefore, the aging costs are too high, no electric motor usage will be allowed, and only the combustion motor will be used. The temperature increase of the cell due to the demand of the electric motor torque is based on the lumped mass thermal model described earlier. It considers the actual cell operation and delivers the aging-relevant temperature, see Eq. (4). The equation uses cell-specific parameters for the resistance, surface, mass, and specific heat capacity. The electric current causes a temperature increase if the heat dissipation according to the cooling is too small. An air-cooling system like in a similar vehicle integration is assumed for the thermal simulation in the operating strategy.

$$\Delta T = \frac{I^2 \cdot R_{\mathrm{Batt}}(T) - k \cdot A_{\mathrm{Batt}} \cdot \left(T_{\mathrm{Batt}} - T_{\mathrm{amb}}\right)}{m_{\mathrm{Batt}} \cdot c_{\mathrm{Batt}}} \cdot \Delta t, \tag{4}$$

with ΔT is the battery temperature increase in K, I is the battery current in A, $R_{\mathrm{Batt}}(T)$ is the temperature dependent resistance in Ω, A_{Batt} is the battery surface in m^2, k is the heat transfer coefficient in $\mathrm{W\,m^{-2}\,K^{-1}}$, T_{Batt} is the battery temperature in K, T_{amb} is the ambient (coolant) temperature in K, m_{Batt} is the mass of the battery in kg, c_{Batt} is the specific heat capacity in $\mathrm{J\,kg^{-1}\,K^{-1}}$, Δt is the calculation time step in s.

Figure 2 shows an example of the methods use at a specific torque request during a worldwide harmonized light-duty vehicles test cycle (WLTC) from the test bench measurements. These diagrams compare the basic operating strategy without any aging consideration with the

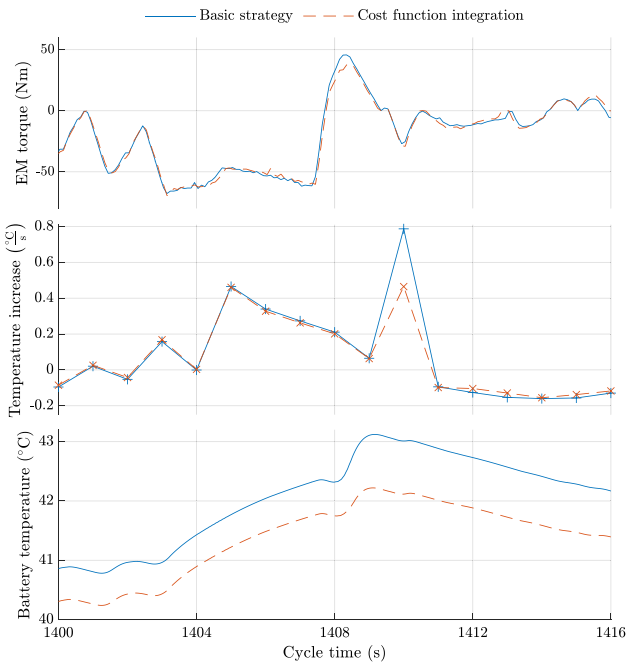

Fig. 2 Intervention of Method A (the cost function integration method) in a torque request compared to the basic strategy, torque (above), temperature rise (middle) and battery temperature (bottom)

Method A. The intervention reduces the electric motor torque (top diagram) only at the load change at around 1408 s because the temperature rise (middle diagram) would be too high. This results in a lower battery temperature rise after the torque request, bottom diagram. Generally, this method allows for considering aging effects within the cost minimum search and will reduce the torque on occasions with high aging potential. Thus, the operating strategy can optimize a driving situation to reach low fuel consumption and reduce battery aging. However, a potential disadvantage is the need for a thermal simulation at each of the multiple calculated torque values within one cost function time step. Such additional calculation can be challenging in real-time applications because engine control units (ECU) have only limited computation power.

– Method B: motor torque limits dependent on the state of health. The second developed and tested active consideration method is based on reducing the electric motor torque dependent on the state of health (SoH). The main idea is to calculate engine limits according to the deviation between the actual SoH compared to a planned SoH. For example, such a planned SoH could use an allowed percentage decrease at a certain timespan or more complex ones. Figure 3 shows the basic derivation of the maximally allowed torque request, which limits the motor (positive limit) and generator (negative limit) operation based on the actual aging state. Based on the

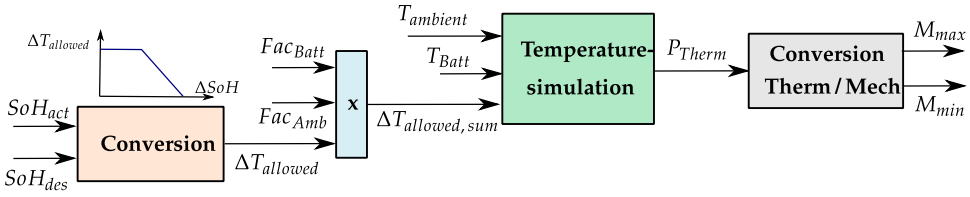

Fig. 3 Schematic of the conversion between aging state and motor torque limits

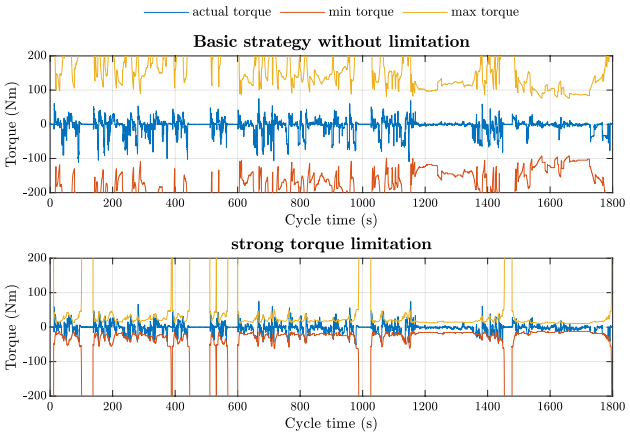

Fig. 4 Example of a strong torque limitation resulting based on a high ΔSoH compared to the basic operating strategy (above)

SoH difference, a maximally allowed temperature rise is calculated. Two influence factors Fac_{Batt} and Fac_{Amb} are used to consider the absolute temperatures of the battery and the ambient. The result is in an overall maximum temperature rise as input for the thermal simulation. This model is the same as shown in Eq. (4) and provides the maximum thermal power loss of the battery. This thermal power can be converted into torque limits of the electric motor using the battery and e-motor efficiencies. Figure 4 shows an example of this electric torque limitation. The diagram shows a comparison of the actual torque and its limits for the basic operating strategy (upper diagram) and an excessive (stronger than regular use) limitation of the torque (bottom diagram) during a WLTC, for example, a high difference between actual and planned SoH. The occasional exceeding of the actual torque in the lower diagram at the strong limitation is based on dynamic torque requests that temporarily overrule the basic operating strategy within the dynamic power limits of the battery. Advantages of this consideration method are the possibility for a layout as a control loop with the actual SoH and the single temperature calculation at every time step. On the negative side, a limitation of the negative motor torque (recuperation) always leads to higher fuel consumption because of less braking energy recuperation. The result is a trade-off between fuel consumption and battery lifetime.

2.2.2 Considerations of battery aging during the powertrain design

Another possibility of considering the battery aging in a hybrid system is using the knowledge on aging to design the powertrain system better concerning the battery and electric motor size as well as crucial operating parameters. For example, with a low influence of the battery C-rates, the battery capacity can be reduced to save costs. Changes like this and parameter changes of the operating strategy are topics of the powertrain design process and can only be simulated using a longitudinal vehicle model. The basis for such a model in this study is a regular C-segment car with a 1.4 l-SI-engine, a 7-gear automatic transmission, and a 48 V mild hybrid system with the investigated battery cells. Such a simulation calculates the actual battery current and the fuel consumption due to the current driving demand due to a driving cycle, in this case, the WLTC.

Investigating the impact of design changes is done by simulation and comparison of different setups. Four different designs are analyzed and their influences on battery aging are evaluated:

1. Design 1 $C_{80\%}$—slight reduction of the battery capacity by 20% for lowering the battery costs.
2. Design 2 $C_{50\%}$—a stronger reduction of the battery capacity by 50% for lowering the battery costs even further. Although just the usable SoC-range of the operating strategy would be needed, the capacity reduction is limited to half of its original value to limit the resulting C-rate surpassing the technical maximum of the cell.
3. Design 3 $SoC_{40\%}$—lowered mean SoC from 50% to 40% to reduce aging.
4. Design 4 $SoC_{40\%}$ & $C_{80\%}$—combination of a 20% capacity reduction with a lowering of the mean SoC to 40%.

Essential for achieving the same fuel consumption and, therefore, comparability for each capacity reduction, the depth of discharge (the difference between SoC high and

Table 2 Parameters of the hybrid system during the different investigations

	Basis	Design 1 $C_{80\%}$	Design 2 $C_{50\%}$	Design 3 $SoC_{40\%}$	Design 4 $SoC_{40\%}$ & $C_{80\%}$
DoD	30%	37.5%	60%	30%	37.5%
SoC_{mean}	50%	50%	50%	40%	40%
Battery capacity	100%	80%	50%	100%	80%
DC-resistance	100%	125%	125%	100%	125%

low) needs to be widened, affecting aging. If this is not done, lesser usable capacity is available and the fuel consumption is increased. Also, a 25% higher DC-resistance is assumed to cover the worst-case by changing the electrochemical parameters to achieve the capacity reduction. All parameters during these investigations are summarized by Table 2.

2.2.3 Test bench measurements

For validating both active aging consideration methods, they were integrated into the operating strategy of a 48 V-mild hybrid system. For the validation of the model, driving cycle measurements on a hardware in the loop engine test bench were used. A regular 7-gear automatic transmission C-segment car was the simulated load for the turbocharged 1.4 l-SI-engine combined with a mild hybrid system, including a boost recuperation motor of about 10 kW from Bosch. The power supply unit at the test bench was used, simulating a comparable lithium ion battery pack of the hybrid system. It included the aging model for the investigated cells in Sect. 2.1.1. The basic operating strategy relied on an ECMS. The results were compared to the basic operating strategy.

As benchmark parameters for the impact of both methods, the fuel consumption and the capacity loss during the driving cycle were used. The engine fuel consumption is measured using a mass flow meter and is accumulated to an overall mass. State of charge deviations at the end of the cycle must be considered for the overall fuel consumption during the driving cycle. For the conversion, an average efficiency for the internal combustion engine was used to calculate the needed fuel to generate the SoC change. The second benchmark criterion is the impact on battery aging with the overall capacity loss of a new cell during the driving cycle (aging time 1800 s). This value is calculated with the developed aging model in Eq. (7) based on battery usage during the cycle.

All measurements represent a comparison between the basic strategy and one of the described intervention-methods in a representative driving cycle. For each variant, the strength of the intervention can be influenced using a factor (Fac_{SoH}) in the cost function integration method to increase the aging costs in the ECMS or the SoH difference in the limitation method for reduced torque limits. Besides these variations, several tests were also conducted at different ambient temperatures (5, 30 and 50°C) to investigate the temperature dependency.

3 Results and discussion

3.1 Aging investigations

The lithium-ion battery aging generally leads to capacity loss and resistance rise. Both parameters can serve as an expression for the actual battery aging state SoH. The end-of-life requirements for batteries differ from one manufacturer to another. In the automotive industries, most companies determine a remaining capacity of 70–80% or a resistance increase of at least 100% as their end-of-life criterion. Besides these two parameters, a maximum charge throughput is often used in terms of simplicity because no capacity or resistance measurement is needed.

An example for capacity loss is shown in Fig. 5. Each line displays the mean value for the capacity loss of both tested cells at the same condition during the cycle tests as a function of the measurement time for the tests at a cooling fluid temperature (and therefore the case temperature) of 50°C. The capacity loss is referenced to the initial capacity measurement of each cell at its begin-of-life after formation. This method is used for resistance as well. The data represents the weekly checkup cycle results. The reason for the shorter measurement time at 25 C is the limited amount of higher current test channels because of which the tests are run one after the other.

Using this diagram, it is possible to compare the calendar and the cycle aging. The fact that cells at 1 C are aging faster than the calendar aging cells at 0 C is attributed to the higher

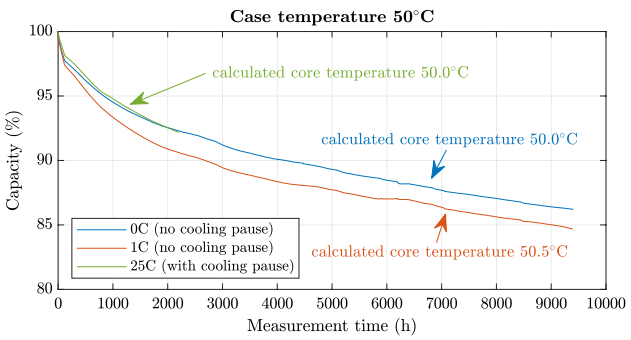

Fig. 5 Capacity loss over the measurement time for an ambient fluid temperature of 50°C with the calculated mean core temperatures

core temperatures caused by the current. The high C-rates (e.g., 25 C), however, only show an aging process like the 0 C-storage tests. This inconsistent aging is caused by the resulting cell core temperatures. This temperature is slightly higher at the small C-rate, while for the high C-rate, it is on the same level as the storage test because of the cooling pauses between cycles. A detailed investigation is done in Sect. 3.1.2 by shortening this pause time to gain the relevant temperature responsible for aging. The calculated core temperatures for each test according to the thermal model are also included in Fig. 5. No cell reached the end-of-life criteria during investigations. The highest charge throughput was around 100 kAh corresponding to roughly 12,500 full cycles.

The resistance results show no consistency, especially at the high C-rate tests, contrary to the capacity loss. Figure 6 displays the data for the 3 C- and 10 C tests at various temperatures. The 10 s-DC-resistance generally rises over the whole investigation time but varies most likely due to the measurement tolerances (voltage drop after 10 s) based on ambient temperature deviations combined with the relatively small level of about 1–2 mΩ.

For example in the diagram of Fig. 6a the data for the 3 C cycled cells at different ambient temperatures of 5, 25 and 35°C is shown. The highest cell resistance rise is around 20% and the average below 10%. The 10 C-data, for example, in Fig. 6b shows more scattering with even a resistance drop. In general, the power loss due to the resistance rise during the investigations is relatively small, with most data below 2%. The charge power loss is equal to the shown discharge power loss. Both power losses are calculated for the 3 C-current pulse at the DC-resistance capturing. The capacity loss demonstrates a better reference and is, therefore, used for the modeling of the battery aging.

3.1.1 Calendar aging

3.1.2 Temperature and time influences

The calendar aging occurs throughout the lifetime of lithium-ion cells. For parameterizing an Arrhenius model, the storage tests without charging are used. Due to the scattering and a possible outlier at the 5°C test (lower right data point in Fig. 7b) of the 0 C-data also the 1 C cycling tests are taken into account. This adding of data samples is done for repeatability, although the minor core heating causes a slight error due to the 1 C-current.

The Arrhenius equation with the extension of the aging time is a well-known method to describe the calendar aging [1, 4]. The calendar aging of lithium-ion batteries is proportional to the square root of time [19], which is confirmed by the test data in Fig. 7a. If an Arrhenius behavior is present, the function represents a straight line in the so-called Arrhenius plot shown in Fig. 7b on the right-hand side. This diagram has the inverse temperature on the horizontal axis and the logarithmic capacity loss on the vertical. The Arrhenius plot is also used to parameterize the pre-exponential factor a and activation energy E_A of the aging model in Eq. (5). In the Arrhenius diagram of Fig. 7b the capacity loss of each cell after 217 days is plotted and the linear fit is used to determine the unknown pre-exponential factor a and the activation energy E_A in Eq. (5) of the Arrhenius-model. They result in the cell-specific values of $a = 6972.5$ and $E_A = 24{,}204\,\mathrm{J\,mol^{-1}}$.

$$C_{\mathrm{Loss}} = a \cdot \sqrt{t} \cdot \exp\left(-\frac{E_A}{R \cdot T}\right) \tag{5}$$

with C_{Loss} is the capacity loss to C_{init} in %, a is the pre-exponential factor, t is the aging time of the cell in days, E_A is the

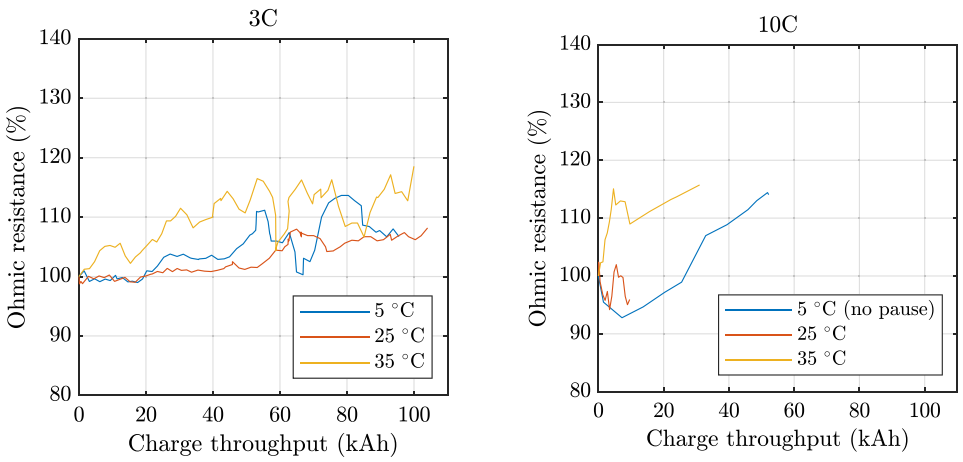

(a) 3C **(b)** 10C

Fig. 6 Mean values of the 10 s-DC-resistance change for the lithium-ion cells over the charge throughput for the 3 C- and 10 C-tested cells

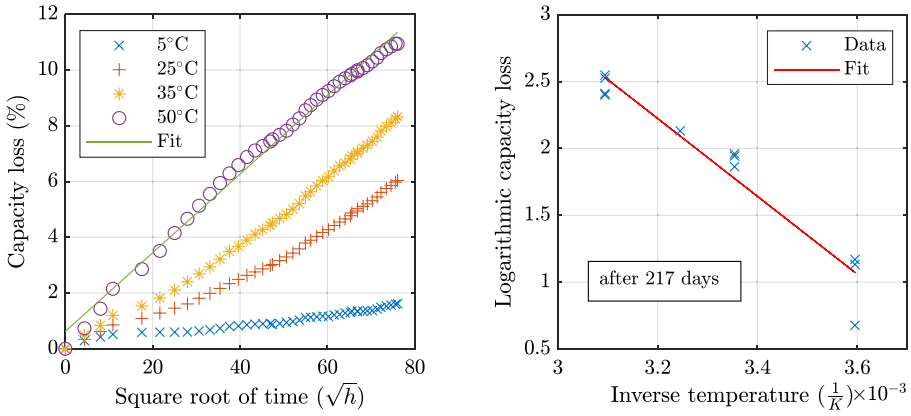

Fig. 7 Investigation of the time and temperature dependency of the calendar aging

(a) Time dependency of the calendar aging test

(b) Arrhenius plot after 217 days for calendar aging data of the 0C & 1C-tests

activation energy in J mol^{-1}, R is the universal gas constant J kg^{-1} K^{-1}, T is the temperature of the cell in K.

3.1.3 State of charge influence

The SoC influence is another focus of these investigations. Storage tests at different SoC levels between 10 and 100% represent the input data for this dependency investigation. The results of these tests are shown in Fig. 8a. For comparison, only the linear aging phase and its gradients are of interest in this investigation. The later start was used to skip the exponential aging phase at the beginning of the life of each cell. This new starting point for each cell is the reference value, so each starts at a capacity of 100%. A small SoC value does not lead to any aging in the time frame of these storage tests, while stronger aging can be observed at higher SoCs. The order of all curves correlates with the SoC levels except for the cell at 90%. This cell seems to be an outlier.

The diagram in Fig. 8b shows the gradients for each SoC level of the left-hand side data and uses it to model the SoC influence. Without any further measurements to clarify any outliers or normal scattering of the high SoC data points (90 and 100% SoC), both are included in the fitting process to minimize the possible error of a wrong decision. An exponential function seems to be the best solution. The fit is also shown in the diagram. Equation (6) describes this function for the influence factor α_{SoC} using both pre-factors for the fitting.

$$\alpha_{\mathrm{SoC}} = \frac{b_1 \cdot \exp\left[b_2 \cdot (\mathrm{SoC})\right]}{\alpha_{50\%\,\mathrm{SoC}}} = \exp\left[b_2 \cdot (\mathrm{SoC} - 50)\right] \tag{6}$$

with α_{SoC} is the SoC influence factor, b_1 is a pre-factor, b_2 is the pre-factor in the exponential function for the SoC = 0.024, SoC is the state of charge in % (50% = 50).

To be able to integrate this description into an aging model, it needs to be referenced to the other tests which were conducted at an SoC of 50% ($\alpha_{50\%\,\mathrm{SoC}}$). The result is

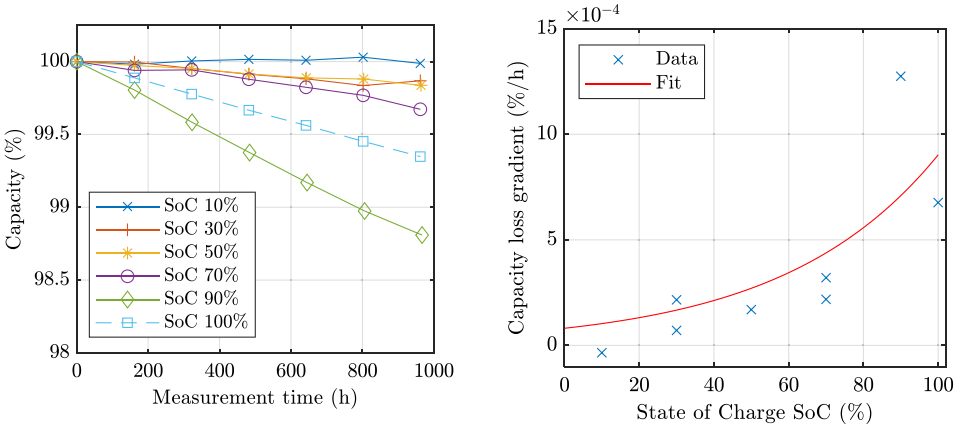

Fig. 8 State of charge dependency investigation with storage data at 23°C

(a) Capacity loss data

(b) Capacity loss gradient modeling

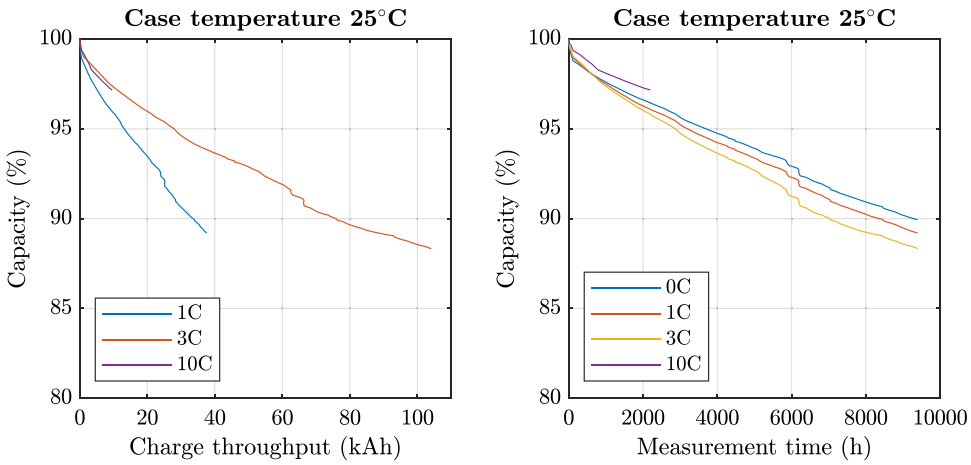

(a) Charge throughput **(b)** Measurement Time

Fig. 9 Aging due to cycling of the cell at an ambient fluid temperature of 25°C

the final formula shown in Eq. (6). This modeling is not capable of considering lithium plating or any cycling-based aging effects as no cycling was done in the state of charge influence investigations.

3.1.4 Cycle aging

The cycle aging was the main focus of the investigations. Several test conditions were used to analyze the C-rate dependency at different temperatures. The capacity losses, for example, in Fig. 5 show only a similar aging behavior to the storage tests for cases where a sufficient cell cooling and long pauses to regain the starting battery temperature are used. The first finding in this context is that temperature is the predominant effect for aging under these conditions. At the cycle tests, the additional current contribution results in a temperature rise of the cell due to the resistive current losses. This higher cell temperature cause higher aging losses. But the efficient cooling at the test bench combined with long pauses can prevent any temperature elevation. In this context, no additional current effects on aging were found except the temperature. This assumption can be shown with a comparison of the capacity loss over charge throughput and the measurement time in Fig. 9.

The capacity data are plotted over the charge throughput on the left-hand side diagram of Fig. 9a to see the impact of the C-rates on the aging state at an ambient fluid temperature of 25°C. There the 1 C-test shows the strongest aging during the investigations and both others have a much flatter curve. Contrary to this diagram, Fig. 9b shows the same data over the measurement time with a nearly inverted order except for the 10 C-test with the cooling pause. This indicates that the temperature is the most significant impact on aging if the cell cooling is sufficient. The cells at the higher C-rate achieve more charge throughput in the same period between the weekly checkups than the smaller C-rate tests. Such a behavior is also assumed by Schmidt in [21] for the tested coin cells. There is a strong indication that the significant contribution of cycling to battery aging is through additional cell heating due to the losses and, therefore, faster aging.

3.1.5 Aging-relevant cell temperature

This independent test examines the previous assumption in more detail and determines the representative temperature value for the whole aging losses in the cell at this condition. This test compares the measured with the modeled aging based on a constant temperature. The resulting temperature is called aging-relevant temperature and will be used as input for the aging model. Especially during operation at high C-rates, the inner thermal distribution is very inhomogeneous and the aging-relevant cell temperature needs to be identified. The test for this temperature is done at a single condition with a charge rate of 10 C and 35°C ambient fluid temperature. The choice of this condition is based on testing equipment availability. As an indication also the mean electrode temperature all along one test cycle (charging and discharging) is used. A simulation describes the mean core temperature during operation.

With the assumed current dependency only by cell heating, it would be possible to model the capacity loss solely with the actual battery temperature and this temperature can be increased with a shortening of the pause time. So in the first step, the initial long pause of 10 min is reduced to 4 min. This results in a minor increase of the core and mean electrode temperature to about 37°C. In the last step, this pause time is deleted, which elevates the mean electrode temperature to about 46°C and the modeled core temperature to 44°C. This is leading to a significant temperature difference between the surface (ambient) and the core. The bottom diagram of Fig. 10 summarizes the temperature changes in every step for the pause reduction.

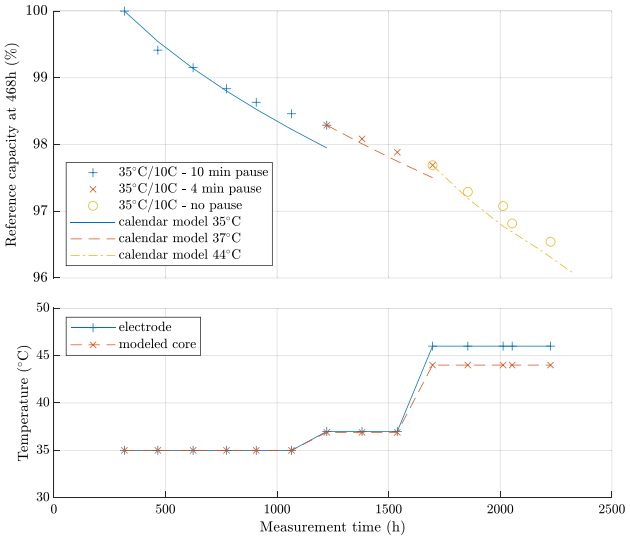

Fig. 10 Cooling pause variation at 10 C and 35°C coolant temperature (case) with its comparison to the aging model in upper graph and temperatures in lower graph

The upper diagram of Fig. 10 shows a comparison of the modeled and measured aging losses. The test is separated into the three different phases for 10 min in blue, 4 min in red, and no pause in yellow. The diagram shows the recurrent checkup cycle tests as data points and the simulated aging processes according to the aging model for each temperature as curves. In this diagram, the exponential loss at the beginning of battery aging is excluded, and the chart focuses just on the linear progress later on. Hence, an equal comparison between all three steps is easily possible. The curve starts at 468 h with a referenced capacity of 100% at this measurement time. The measurement data and the model show a good correlation. This test demonstrates the importance of an accurate simulation of the core temperature at high C-rates and the use of the core temperature instead of the ambient or the case temperature for aging simulations. It is possible to calculate the capacity loss as a function of the calculated battery temperature.

3.1.6 Aging model

A final aging model was developed by summarizing all single investigations, Eq. (7). The model calculates the capacity loss of the cell based on the temperature and the SoC. The cells aging history is also essential at using this model because the aging process flattens according to the square root of time. With an accurate temperature model, it is also possible to calculate dynamic load profiles.

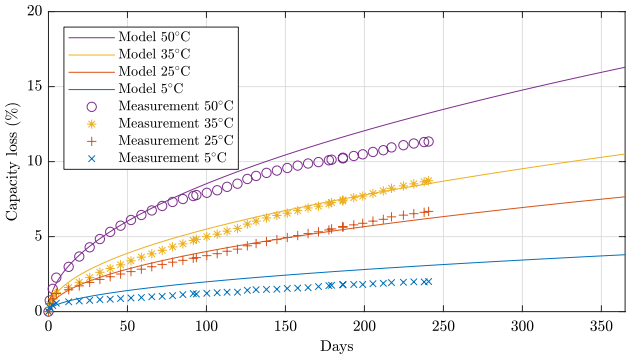

Fig. 11 Comparison of the calendar aging test data and the aging model

$$C_{\text{Loss}} = a \cdot \sqrt{t} \cdot \exp\left[-\frac{E_{\text{A}}}{R \cdot T} + b_2 \cdot (\text{SoC} - 50)\right] \tag{7}$$

with C_{Loss} is the capacity loss to C_{init} in %, a is the pre-exponential factor = 6972.5, b_2 is the factor for SoC deviation = 0.024, SoC is the state of charge in percent (50% = 50), t is the aging time of the cell in days, E_{A} is the activation energy = 24,204 J mol^{-1}, R is the universal gas constant 8.314 J kg^{-1} K^{-1}, T is the temperature of the cell in K.

Finally, a comparison between model and measured calendar aging data is illustrated in Fig. 11. Cell variabilities mainly cause the differences in this diagram at the low and high temperatures. Those deviations can also be seen in the right-hand side diagram of Fig. 7 between the straight fit curve and the data points, especially for the low ambient temperature of 5°C on the right lower side of the diagram. The model can be used in two different ways, calculating the time to cell end-of-life at a specific ambient temperature (30% capacity loss) or calculating the maximally allowed temperature for reaching the desired lifetime. As an example, to achieve a lifetime of 10 years, no higher ambient temperature than 31.7°C is allowed.

Summing up the aging investigations, the aging of automotive high power cells at high charge rates is highly dependent on the core temperature of the cell and not the surface/ambient temperature. The C-rate influence during cycling causes cell heating due to the battery current and higher temperatures lead to faster aging. Another significant influence on battery aging is the state of charge, where high levels cause strong battery aging.

3.2 Aging considerations in a hybrid system

3.2.1 Aging considerations during operation

The main focus of aging consideration for hybrid systems in this paper is during the operation. For this, the model is integrated into the hybrid operating strategy and considers

the aging during the vehicle driving control the battery's aging process. Two different methods were developed in this research to achieve control of the aging process (Method A for the integration into the cost function of an ECMS operating strategy and B for the torque limitation as described in Sect. 2.2.1). Both were integrated into the operating strategy of a 48 V mild hybrid system and were tested on an engine test bench. All following data was gathered during driving cycle tests. Comparisons between the basic operating strategy without any aging consideration and both presented methods show the respective potential for aging reduction while preserving fuel consumption savings. The aging is calculated using the aging model in Eq. (7). The crucial usage parameters are the temperature and the state of charge. Figure 12 shows their values during an 1800 s long WLTC for both variants (yellow Method A cost function integration and red Method B torque limitation) compared to the basic strategy (blue).

The most obvious fact is the large difference between the battery temperature in the basic strategy (blue) and the strong torque limitation (red) during the whole driving cycle. This lower temperature indicates a lower battery aging compared to the basis. Similar to the temperature, the SoC is also lower for the torque limitation method than with the basic strategy. The aging integration into the cost function shows nearly unnoticeable temperature and SoC changes than the basic operating strategy. Both input parameters influence the capacity loss against the initial capacity during a driving cycle with the aging time of 1800 s. The best way of comparing all methods to the basic strategy is by analyzing the overall capacity loss and the consumed fuel during a WLTC. Figure 13 summarizes all WLTC measurements at an ambient air temperature of 30°C for each method and all strength variations (different prefactors $\mathrm{Fac}_{\mathrm{SoH}}$ and ΔSoH) of each one. The torque limitation variant allows a strong aging

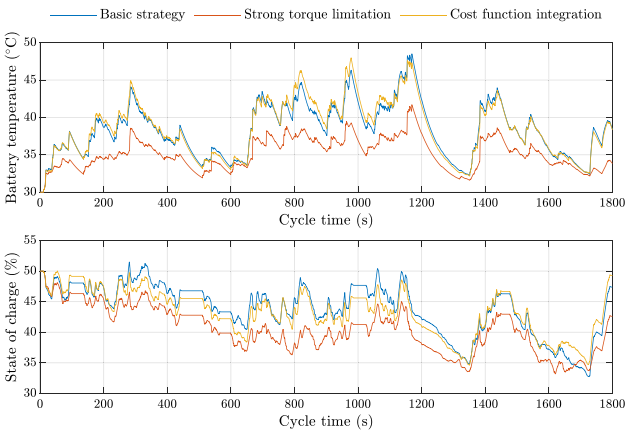

Fig. 12 Comparisons between the basic strategy and both active consideration methods for the battery temperature (above) and the state of charge (bottom)

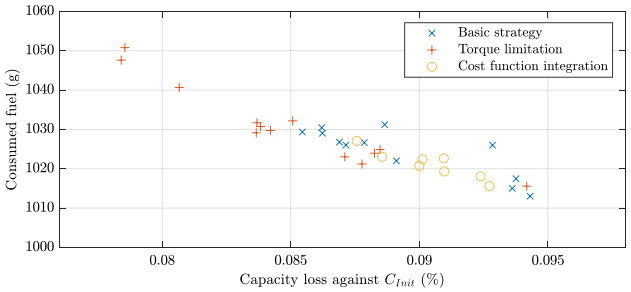

Fig. 13 Test bench data of fuel consumption and capacity loss during a WLTC at 30°C ambient air temperature for the different operating strategy variants

reduction at some levels of variation. In contrast, the integration of aging in the cost function reaches no significant reduction of battery aging compared to the basic strategy.

- Method A: aging integration into the ECMS cost function. The method of integrating the battery aging into the ECMS operating strategy cost function reaches nearly no reduction of the capacity loss or fuel consumption because all results are inside the measurement tolerance of 1%. All data points for the integration method in Fig. 13 are the results of a variation of the aging cost prefactor $\mathrm{Fac}_{\mathrm{SoH}}$ in Equation (3) between 1 and 5 for varying the method strength. This results in aging costs multiple times the overall costs without aging. Like already indicated in the temperature and SoC comparison (Fig. 12), the main reason for the low aging reduction is the failed lowering of the mean battery temperature during the cycle. A reason why method A is not suitable for a significant temperature reduction is that the operating strategy does not limit the hybrid system's recuperation power with its high currents. Since energy is stored in the battery during recuperation, even a high aging cost prefactor $\mathrm{Fac}_{\mathrm{SoH}}$ for the electrical energy does not limit the charging power. Therefore, in addition to limiting the boost power, this method would have to be expanded to include a limitation of the recuperation power. Besides the low impact, it might be problematic to integrate an accurate thermal simulation into a real-time optimization in an engine control unit with its limited calculation performance.
- Method B: motor torque limits dependent on the state of health. The second method of limiting the electric torque dependent on the aging state delivers better results with a significant aging reduction confirmed by the measurements shown in Fig. 13. The selected difference values between the actual and planned SoH at this test result in a strong varying of the torque limitation for the electric motor. The value selection for these measurements was made solely regarding reaching a different limit. With the

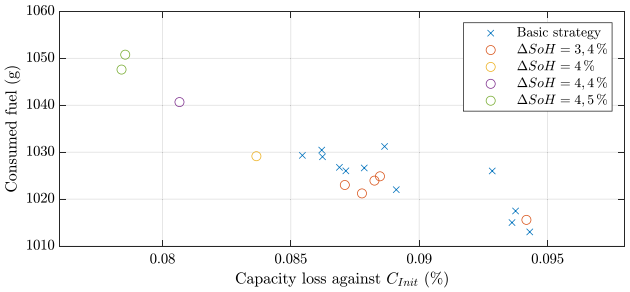

Fig. 14 Detailed analysis for the different strength variations of the SoH dependent limitation method with the fuel consumption and capacity loss during a WLTC at 30°C ambient air temperature

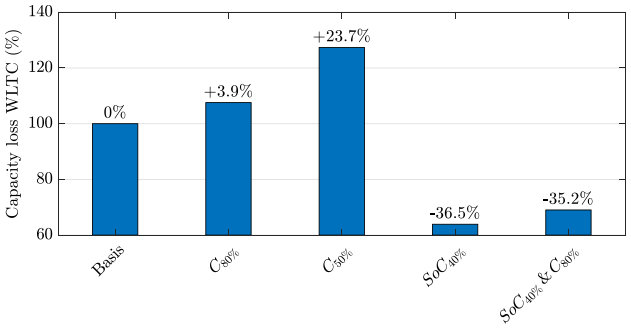

Fig. 15 Comparison of the simulation results for the capacity loss against a new cell during a WLTC for different hybrid powertrain design variants

wide variation of the restriction, the data shows a wide range of measurement points. The diagram in Fig. 14 displays the different limitation strengths for a more detailed analysis. A higher ΔSoH means a stronger limitation. For example, the strong variant in Fig. 4 has a ΔSoH of 4.5% resulting in a limitation of the electric motor torque to a maximum of about 30% compared to the unrestricted basis. A trend can be seen that a stronger limitation (higher ΔSoH) leads to decreased capacity loss. But this aging reduction can only be achieved at the cost of higher fuel consumption. The cause of this higher consumption is a decreased use of the electric motor during recuperation and boosting. Therefore the combustion engine operation is needed more often. But this reduced use of the electric motor also lowers battery heating and results in a lower mean temperature. Figure 12 shows the strong limitation case (ΔSoH = 4.5%) and the resulting significantly lower temperature compared to the basic strategy. Consequently, this method allows to actively control the aging process during operation. However, because of the higher fuel consumption, it is not suitable to use this operating strategy function throughout the lifetime of the hybrid system rather than activate it just in times of excessive aging. For example, high ambient temperatures protect the battery and remain at the standard ECMS otherwise.

3.2.2 Aging considerations in the powertrain design

The knowledge of the battery aging influences can also be considered in the powertrain design. The results of longitudinal vehicle simulations for different layout versions according to aging considerations are shown in Fig. 15.

The reference of all data is the basic design with its original operating strategy without any aging consideration. The four investigated variants in this diagram are $C_{80\%}$ for the slight capacity reduction of 20%, $C_{50\%}$ for the strong reduction by half, $SoC_{40\%}$ for the lowering of the mean SoC by 10%, and $SoC_{40\%}$ and $C_{80\%}$ for the combination of a lowered SoC with a slight capacity reduction. The effects on DoD and C-rate are already described in Sect. 2.2.2.

Summarizing this chart, massive reductions of aging are possible if the state of charge is lowered by 10% due to the exponential SoC-influence. Of course, a higher reduction would be more beneficial, but a lower SoC also means lower maximum power due to the lowered voltage. This lower voltage in this example leads to a lowered maximum battery pack power of around 100 W (about 0.8%) at the cells maximum current of 300 A. Contrary to this considerable reduction of aging compared with $SoC_{40\%}$, both smaller battery capacity variants show stronger aging. This higher capacity loss is caused mainly because of the wider DoD range for achieving an equal fuel consumption. But both smaller batteries allow fewer battery costs than the origin. Also disadvantageous at the $C_{50\,\%}$-variant are the high resulting charge rates above 50 C due to the reduced capacity whereby cell charge rate limits are exceeded.

The best solution for this investigation is a combination of a slight battery capacity reduction with a lowering of the SoC by 10%. It saves battery costs and has a substantial aging reduction potential, although lower than the SoC-reduction variant. Besides the decreased aging, the reduction in maximum power because of the lowered state of charge has to be kept in mind.

4 Conclusion

The aging investigations in this research concentrated on the battery aging of high power lithium-ion cells designed for automotive use in mild hybrid systems. The main influences SoC, temperature, and C-rate on aging were investigated by aging the cells at defined conditions on a designated test bench. The main finding was a strong influence of the cell core temperature on the aging behavior of these cells. The only influence of the current flow on aging is based on the cell heating due to the resistance losses and the higher aging due to the

higher temperature. This is shown by calculating the battery aging solely with the actual cell core temperature. Another investigated dependency for battery aging was the state of charge during cell storage. Here the known aging influence of a high SoC causing faster aging was confirmed. An aging model capable of describing the main influences of temperature and SoC for such automotive high power cells was developed by using the investigation results.

The developed aging model in the current research work was integrated into the operating strategy of a mild hybrid system for considering battery aging. There are two possible ways to consider aging. On the one hand, during battery usage, aging can be influenced by controlling operational parameters. On the other hand, the gained information on aging can be used to optimize the design of the powertrain. Two different methods in the hybrid operating strategy were developed to influence the battery aging process during operation. One approach integrates an aging function into the cost function of an ECMS operating strategy. This method avoids conditions of high aging potential to reach the desired lifetime. The other method limits the electric motor's torque dependent on the difference of the actual compared to the planned aging state to minimize aging if needed. Both active variants were integrated into the operating strategy of a real 48 V mild hybrid system for validation at a test bench. Only the method with a torque limitation dependent on the SoH achieves controllability of the battery aging process but at the cost of higher fuel consumption. One suitable way of using this method is as a safety feature with limitation of the battery use in extreme situations, for example, at high ambient temperatures. Then this method can prevent the battery from excessive aging. Besides the active methods, the knowledge of the aging influences can be used to improve the hybrid powertrain design. It shows that the best solution for the calculated example is to decrease the mean state of charge and to reduce the battery capacity slightly for achieving significant aging reductions combined with lower battery costs.

Funding Open access funding provided by TU Wien (TUW). This project has received funding from the Mobility of the Future programme Grant Number 854935. Mobility of the Future is a research, technology and innovation funding programme of the Republic of Austria, Ministry for Climate Action. The Austrian Research Promotion Agency (FFG) has been authorised for the programme management.

Declarations

Conflict of interest The authors declare that they have no conflict of interest.

References

1. Barré, A., Deguilhem, B., Grolleau, S., Gérard, M., Suard, F., Riu, D.: A review on lithium-ion battery ageing mechanisms and estimations for automotive applications. J. Power Sources **241**, 680–689 (2013). https://doi.org/10.1016/j.jpowsour.2013.05.040
2. Bernardi, D., Pawlikowski, E., Newman, J.: A general energy balance for battery systems. J. Electrochem. Soc. **132**(1), 5–12 (1985). https://doi.org/10.1149/1.2113792
3. Broussely, M., Herreyre, S., Biensan, P., Kasztejna, P., Nechev, K., Staniewicz, R.: Aging mechanism in Li ion cells and calendar life predictions. J. Power Sources **97**, 13–21 (2001). https://doi.org/10.1016/S0378-7753(01)00722-4
4. Broussely, M., Biensan, P., Bonhomme, F., Blanchard, P., Herreyre, S., Nechev, K., Staniewicz, R.: Main aging mechanisms in Li ion batteries. J. Power Sources **146**(1–2), 90–96 (2005). https://doi.org/10.1016/j.jpowsour.2005.03.172
5. Denner, V.: Beyond the hood—rethinking mobility. In: Proceedings of 40th International Vienna Motor Symposium, 15–17 May 2019. VDI-Verlag (2019)
6. Doeff, M.M., Wilcox, J.D., Kostecki, R., Lau, G.: Optimization of carbon coatings on LiFePO4. J. Power Sources **163**(1), 180–184 (2006). https://doi.org/10.1016/j.jpowsour.2005.11.075
7. Dominko, R., Bele, M., Gaberscek, M., Remskar, M., Hanzel, D., Pejovnik, S., Jamnik, J.: Impact of the carbon coating thickness on the electrochemical performance of LiFePO4/C composites. J. Electrochem. Soc. **152**(3), A607–A610 (2005). https://doi.org/10.1149/1.1860492
8. Ecker, M., Nieto, N., Käbitz, S., Schmalstieg, J., Blanke, H., Warnecke, A., Sauer, D.U.: Calendar and cycle life study of Li (NiMnCo) O2-based 18650 lithium-ion batteries. J. Power Sources **248**, 839–851 (2014). https://doi.org/10.1016/j.jpowsour.2013.09.143
9. Hofmann, P.: Hybridfahrzeuge: ein alternatives Antriebssystem für die Zukunft. Springer, Vienna (2014)
10. Kim, D.H., Kim, J.: Synthesis of LiFePO4 nanoparticles in polyol medium and their electrochemical properties. Electrochem. Solid State Lett. **9**(9), A439–A442 (2006). https://doi.org/10.1149/1.2218308
11. Lee, J.H., Lee, H.M., Ahn, S.: Battery dimensional changes occurring during charge/discharge cycles-thin rectangular lithium ion and polymer cells. J. Power Sources **119**, 833–837 (2003). https://doi.org/10.1016/S0378-7753(03)00281-7
12. Lee, S.W., Yabuuchi, N., Gallant, B.M., Chen, S., Kim, B.S., Hammond, P.T., Shao-Horn, Y.: High-power lithium batteries from functionalized carbon-nanotube electrodes. Nat. Nanotechnol. **5**(7), 531 (2010). https://doi.org/10.1038/nnano.2010.116
13. Legrand, N., Knosp, B., Desprez, P., Lapicque, F., Raël, S.: Physical characterization of the charging process of a Li-ion battery and prediction of li plating by electrochemical modelling. J. Power Sources **245**, 208–216 (2014). https://doi.org/10.1016/j.jpowsour.2013.06.130
14. Li, S., Maiterth, J., Senft, S., Hülshorst, T., et al.: Considering the aging of lithium-ion battery in the operation strategy for hybrid commercial vehicles. In: 25th Aachen Colloquium Automobile and Engine Technology, pp. 1245–1260 (2016)

15. Lundgren, H., Svens, P., Ekström, H., Tengstedt, C., Lindström, J., Behm, M., Lindbergh, G.: Thermal management of large-format prismatic lithium-ion battery in PHEV application. J. Electrochem. Soc. **163**(2), A309–A317 (2016). https://doi.org/10.1149/2.09411602jes
16. Meethong, N., Kao, Y.H., Speakman, S.A., Chiang, Y.M.: Aliovalent substitutions in olivine lithium iron phosphate and impact on structure and properties. Adv. Funct. Mater. **19**(7), 1060–1070 (2009). https://doi.org/10.1002/adfm.200801617
17. Nazar, L., Goward, G., Leroux, F., Duncan, M., Huang, H., Kerr, T., Gaubicher, J.: Nanostructured materials for energy storage. Int. J. Inorg. Mater. **3**(3), 191–200 (2001). https://doi.org/10.1016/S1466-6049(01)00026-5
18. Padovani, TM., Colin, G., Ketfi-Cherif, A., Chamaillard, Y: Optimal energy management strategy for a hybrid vehicle provided with a dual electric storage system. In: Proceedings of the IFAC Workshop on Engine and Powertrain Control, Simulation and Modeling (E-COSM'15) (2015). https://hal.archives-ouvertes.fr/hal-01192640
19. Ploehn, H.J., Ramadass, P., White, R.E.: Solvent diffusion model for aging of lithium-ion battery cells. J. Electrochem. Soc. **151**(3), A456–A462 (2004). https://doi.org/10.1149/1.1644601
20. Rao, L., Newman, J.: Heat-generation rate and general energy balance for insertion battery systems. J. Electrochem. Soc. **144**(8), 2697–2704 (1997). https://doi.org/10.1149/1.1837884
21. Schmidt, A., Smith, A., Ehrenberg, H.: Power capability and cyclic aging of commercial, high power lithium ion battery cells with respect to different cell designs. J. Power Sources **425**, 27–38 (2019). https://doi.org/10.1016/j.jpowsour.2019.03.075
22. Scrosati, B., Garche, J., Tillmetz, W.: Advances in Battery Technologies for Electric Vehicles. Woodhead Publishing, Cambridge (2015)
23. Serrao, L., Onori, S., Sciarretta, A., Guezennec, Y., Rizzoni, G.: Optimal energy management of hybrid electric vehicles including battery aging. In: Proceedings of the 2011 American Control Conference, pp. 2125–2130. IEEE (2011). https://doi.org/10.1109/ACC.2011.5991576
24. Suri, G., Onori, S.: A control-oriented cycle-life model for hybrid electric vehicle lithium-ion batteries. Energy **96**, 644–653 (2016). https://doi.org/10.1016/j.energy.2015.11.075
25. Vetter, J., Novák, P., Wagner, M.R., Veit, C., Möller, K.C., Besenhard, J., Winter, M., Wohlfahrt-Mehrens, M., Vogler, C., Hammouche, A.: Ageing mechanisms in lithium-ion batteries. J. Power Sources **147**(1–2), 269–281 (2005). https://doi.org/10.1016/j.jpowsour.2005.01.006
26. Waldmann, T., Wilka, M., Kasper, M., Fleischhammer, M., Wohlfahrt-Mehrens, M.: Temperature dependent ageing mechanisms in Lithium-ion batteries—a post-mortem study. J. Power Sources **262**, 129–135 (2014). https://doi.org/10.1016/j.jpowsour.2014.03.112
27. Wancura, H., Weißbäck, M., Silva de Abreu, I., Schäfer, T., Lange, S., Unterberger, B., Hoffmann, S.: From virtual to reality—how 48 V systems and operating strategies improve diesel emission. In: Proceedings of 19th Stuttgart International Symposium, pp 307–316. Springer (2019). https://doi.org/10.1007/978-3-658-25939-6
28. Wang, J., Purewal, J., Liu, P., Hicks-Garner, J., Soukazian, S., Sherman, E., Sorenson, A., Vu, L., Tataria, H., Verbrugge, M.W.: Degradation of lithium ion batteries employing graphite negatives and nickel-cobalt-manganese oxide+ spinel manganese oxide positives: Part 1, aging mechanisms and life estimation. J. Power Sources **269**, 937–948 (2014). https://doi.org/10.1016/j.jpowsour.2014.07.030